Histol Histopathol (2006) 21: 813-821

http://www.hh.um.es

Histology and Histopathology

Cellular and Molecular Biology

Megakaryocytic features useful for the diagnosis of myeloproliferative disorders can be obtained by a novel unsupervised software analysis

C. Tripodo[1], C. Valenti[2], B. Ballarò[2], Z. Rudzki[3], D. Tegolo[2], V. Di Gesù[2], A.M. Florena[1] and V. Franco[1]

[1]Istituto di Anatomia Patologica, [2]Dipartimento di Matematica e Applicazioni, Università degli Studi di Palermo, Italy, and [3]Katedra Patomorfologii, Wydzial Lekarski, Collegium Medicum Uniwersytetu Jagiellońskiego, Kraków, Poland

Summary. An unsupervised method for megakaryocyte detection and analysis is proposed, in order to validate supplementary tools which can be of help in supporting the pathologist in the classification of Philadelphia negative chronic myeloproliferative disorders with thrombocytosis. The experiment was conducted on high power magnification photomicrographs taken from hematoxylin-and-eosin 3 μm thick sections of formalin fixed, paraffin embedded bone marrow biopsies from patients with reactive thrombocytosis or chronic myeloproliferative disorders.

Each megakaryocyte has been isolated in the photos through an image segmentation process, mainly based on mathematical morphology and wavelet analysis. A set of features (e.g. area, perimeter and fractal dimension of the cell and its nucleus, shape complexity via elliptic Fourier transform, and so on) is used to characterize the disorders and discriminate between essential thrombocythemia and idiopathic myelofibrosis. Features related to the general contour of the cell like cytoplasmic area and perimeter are good markers in distinguishing between normal or reactive and pathologic megakaryocytes while nuclear features and global circularity are helpful in the differential diagnosis between ET and prefibrotic IMF. The method proposed should be considered as a fast preprocessing tool for the diagnostic phase and its use can be extended to solve different object recognition problems.

Key words: Megakaryocyte morphology, Unsupervised classification, Morphometry, Chronic myeloproliferative disorders

Offprint requests to: Claudio Tripodo, Istituto di Anatomia e Istologia Patologica, Università degli Studi di Palermo, via del Vespro 129, 90100 Palermo, Italy. e-mail: tripodo@unipa.it

Introduction

Philadelphia-negative (Ph-) chronic myeloproliferative disorders CMPDs are hematopoietic stem-cell disorders which include three main pathological entities namely polycythemia rubra vera (PV), essential thrombocythemia (ET) and idiopathic myelofibrosis (IMF) (Thiele et al., 2001a). In the overt phase of the pathologic processes these diseases show a wide and well-differentiated spectrum of clinical and laboratory features which parallels the different involvement of the three myeloid series into proliferation (Michiels and Thiele, 2002). By contrast, similar and sometimes overlapping clinical pictures can be observed in the early phases of these disorders (Thiele and Kvasnicka, 2003a; Thiele et al., 2005a). Frequently, the presence of a persistent increase of platelet count can be the only sign of an underlying myeloproliferative process (Schafer, 2004). In these cases bone marrow histopathology can be necessary for discriminating different disorders, usually ET from early prefibrotic thrombocythemic IMF, as well as to define the correct prognostic behavior and the most appropriate therapeutic strategies (Thiele et al., 2000, 2002). Recently, immunohistochemistry proved to be a supplementary tool useful in difficult cases and able to add information concerning microvessel density and presence of $CD34^+$ cells (Mesa et al., 2002; Kvasnicka et al., 2004; Thiele et al., 2005b). Due to the different morphologic cytoplasmic and nuclear features of megakaryocytes (MKCs) which characterize the various disorders, morphometric analysis should be taken into consideration as it makes possible the quantitative evaluation of these qualitative data and provides a valid basis for computer-based detection and differentiation tasks (Thiele et al., 1999a). In the present study an unsupervised method for megakaryocyte detection and analysis is proposed which can be of help in supporting the pathologist in the classification of Ph- CMPDs with thrombocytosis.

Materials and methods

Bone marrow trephine biopsies (BMBs) from patients diagnosed with ET (19 cases) and IMF (15 cases), and BMBs from patients with reactive thrombocytosis (18 cases) were retrospectively selected from the archives of the Institute of Pathology, University of Palermo, and Department of Pathomorphology, Collegium Medicum, Jagellonian University, Krakow. All the BMBs had been performed on diagnosis, before any treatment was started, and classified according to the WHO classification criteria. The experiment was conducted on high power magnification (x400) photomicrographs (577x763 pixels) taken from hematoxylin-and-eosin 3µm thick sections of formalin fixed, paraffin embedded BMBs. The digital images were collected under a Leica Leitz DMRB microscope with a Leica PL Fluotar 40x0.70 lens, acquired by a Leica DFC 320 digital camera and processed by a proprietary software developed in MatLab (http://www.mathworks.com). At present our image database contains 102 normal megakaryocytes, 104 ET and 91 IMF cells.

Morphometry gives quantitative measurements of structures with different levels of detail (Ohshima et al., 1995). Starting from the segmented photos we extracted 11 features to describe each megakaryocyte (Table 1) (Beksaç et al., 1997; Coelho et al., 2002). In particular, we computed the area, the perimeter and the fractal dimension of both the whole cell (f_1, f_2 and $f_3=f_1/f_2$ respectively) and its nucleus (f_4, f_5 and $f_6=f_4/f_5$). The area f_7 of the convex hull (i.e. the smallest convex polygon that contains the cell) led to the solidity value $f_8=f_1/f_7$. The eccentricity of the ellipsis which approximates the shape of the cell was stored in f_9. The comparison between the areas of the cell and of its nucleus was considered by the ratio $f_{10}=f_4/f_1$. Lastly, the difference between the contour of the cell and its reconstructed one, obtained by the inverse elliptic Fourier transform with 50 harmonics, was represented by f_{11}. Therefore, the complexity of the contour of the cell was measured by f_3 and f_{11}, as well as the nucleus by f_6, while f_8 and f_9 regarded the global circularity of the cell.

The whole set of such features constituted a distinctive signature of each cell, with 11 floating point values opportunely normalized in [0,1]. This vector can be considered as the cell's coordinates in the 11-dimensional space (Altman, 1999). In order to assign a given cell to its own class, we simply calculated the Euclidean distance in this space between this cell and its three nearest neighbors already classified. The assignment is therefore carried out through a voting strategy among these neighbors. The classifier was a regression tree procedure applied two times: the former to characterize the set of normal megakaryocytes, the latter to distinguish between essential thrombocythemia and idiopathic myelofibrosis.

We noticed that a few features proved better than others when discriminating between pathological and normal megakaryocytes rather than essential thrombocythemia and idiopathic myelofibrosis. In order to verify this, we tested all possible combinations, ranging from just one feature each time to eleven features all together.

Image segmentation

Different steps were required to discriminate the megakaryocytes. A candidate cell had to be located in each given photomicrograph. This phase is called image segmentation since it isolates the cytoplasm and its nucleus. The resulting information was used in the subsequent extraction of the features which return a distinctive signature of each cell. The actual classifier was a regression tree procedure applied on the set of these signatures.

Preprocessing

As images varied greatly in hue/saturation, a normalization was needed. Though the hematoxylin stain is generally lightly purple, we noticed that it was better to convert the images in the grey level space. In our case no information seemed to come from the true color space. In particular, the green and blue histograms of the cytoplasm and of the nucleus were usually overlapped, while the red histogram alone missed some details. Anyway, we carried out a statistical examination of these histograms in order to normalize the images by matching each photo against a representative one.

A technique was developed to divide a given image into three sets of pixels: the cytoplasm, the nucleus and the remaining background. Starting from their typical average grey values, we repeatedly applied a nearest neighbor segmentation on the histogram of the whole image to obtain two stable threshold values $\tau 1$ and $\tau 2$. This approach usually converged quickly and allowed a rough representation of the cells. Indeed, a morphometric study was needed to correctly refine their shapes.

Table 1. The features that characterize each segmented photo.

f_1	cell area
f_2	cell perimeter
f_3	cell fractal dimension
f_4	nucleus area
f_5	nucleus perimeter
f_6	nucleus fractal dimension
f_7	convex hull area
f_8	solidity measure
f_9	ellipsis eccentricity
f_{10}	cell/nucleus ratio
f_{11}	elliptic Fourier measure

Morphological segmentation

Mathematical morphology is a branch of digital image analysis which uses concepts of algebra and geometry (Soille, 2003). Its theoretical foundations have been well established and we are going to recall just the standard terminology. The morphological part of the segmentation process can be sketched by the following sequence of main operations described in Appendix A (Fig. 1).

Wavelets segmentation

The shape of the cell so far obtained was normally well defined, but sometimes we had to improve the edge of the nuclei. The aim of the wavelet transform was the highlighting of structures with different sizes. The underlying theory is simple and the whole process is very fast: the wavelet transform maps the input signal to its coefficients with respect to a basis of wavelet functions, constructed by dilation and translation of another function, called mother wavelet (Grossmann and Morlet, 1984). Different wavelet families make different trade-offs between how compactly the basis functions are localized in space and how smooth they are.

We compared a few discrete implementations for wavelet analysis in order to choose the most appropriate one for our task (Mallat, 1989; Chui, 1992; Daubechies, 1992; Shensa, 1992; Graps, 1995; Cohen and Kovasevic, 1996). We experimentally preferred the *à trous* algorithm which can be seen as a pipeline of isotropic low-pass and high-pass convolution filters (also known as filter bank) (Holschneider et al., 1988). A brief description of this method is given in Appendix B while an example of wavelets to enhance the shape of the nucleus is shown in Fig. 2.

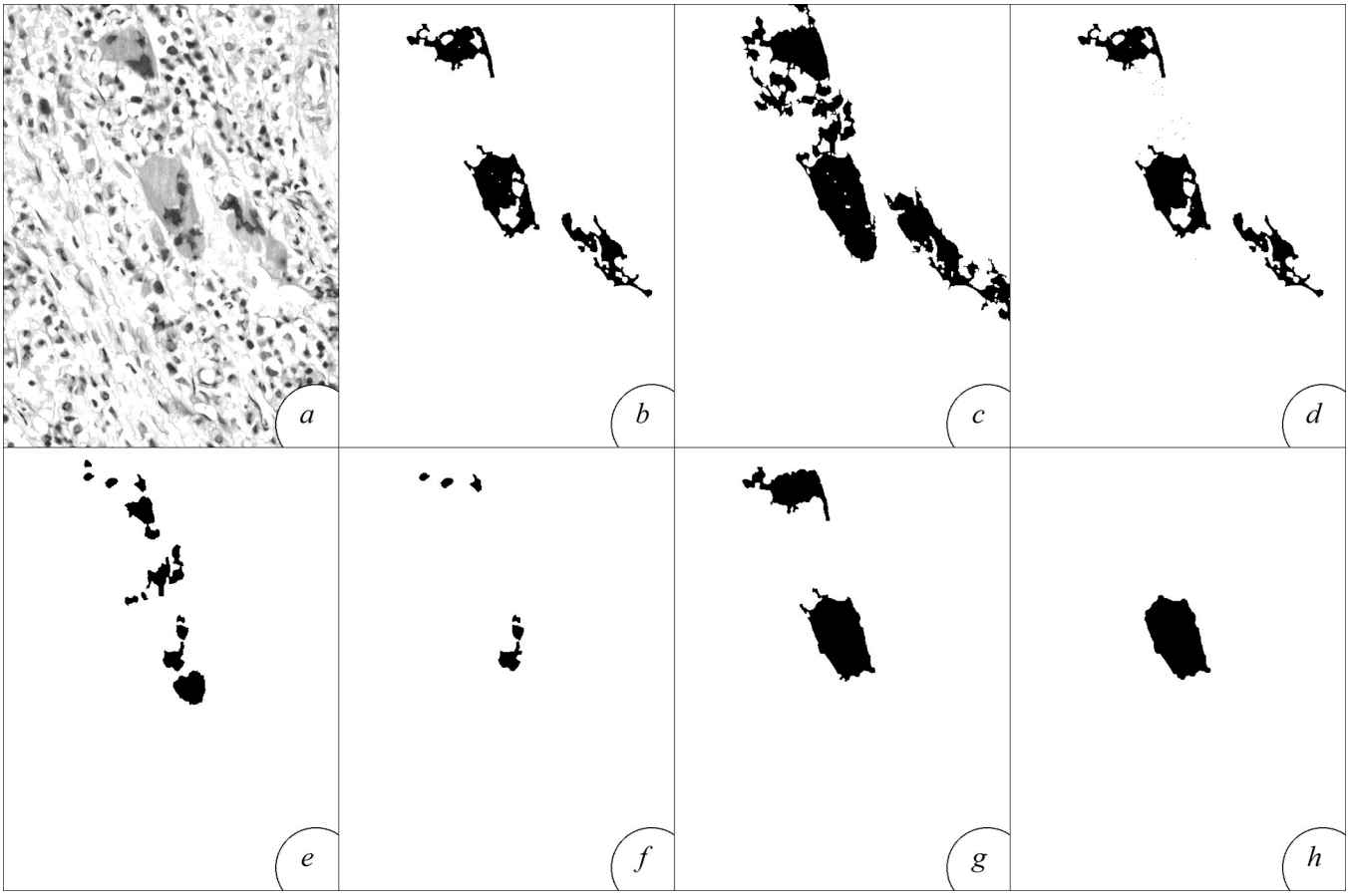

Fig. 1. The segmentation process through mathematical morphology applied to a pathological megakaryocyte **(a-h)**. All naked nuclei have been correctly eliminated **(f)**. Letters refer to the steps described in the algorithm. **a.** enhance the contrast of the dilated grey level image; **b.** create a mask I_{cyto} for the cytoplasm by thresholding the bigger bright areas; **c.** find a mask I_{cell} for the cells by adding the nucleus to the cytoplasm; **d.** the brighter zones within the cell should belong to the cytoplasm; **e.** the mask I_{nucl} of the nucleus lies inside the cell; **f.** remove all possible naked nuclei; **g.** eliminate spurs and smooth the contour of the cell; **h.** get the cell closer to the center of the photo.

Elliptic Fourier descriptors

Due to the discrete lattice, any closed curve can be described as a finite sequence of k points with coordinates (x_i, y_i). The main goal of the elliptic Fourier analysis is to approximate a closed contour as the sum of elliptic harmonics (Kuhl and Giardina, 1982).

This process can be easily inverted to obtain k new points (X_i, Y_i) which should approximate the original contour. Especially for complex contours it is usually necessary to calculate many harmonics to get an accurate enough approximation. Fig. 3 shows an example of elliptic Fourier reconstruction of the contour of a megakaryocyte, by using a variety of harmonics. A slightly formal introduction to the elliptic Fourier transform is in Appendix C.

Results

MKC morphology was normal or well-preserved in reactive conditions, in which MKCs showed round-to-oval shape, normal size of the cytoplasm and multi-lobulated nucleus. In cases of CMPDs, the MKCs often appeared enlarged in size, with over-abundant cytoplasm, irregular shape, and hypo- or hyper-lobulated nucleus. Fig. 4 shows a few examples of cell segmentation.

The confusion matrices relating to the best combination of features, expressed in terms of percentage in Table 2, show that the features $\{f_1, f_2, f_{11}\}$ are suitable for discriminating between pathological and normal megakaryocytes with a sensitivity equal to Se=0.9848 and a specificity equal to Sp=0.9695, while

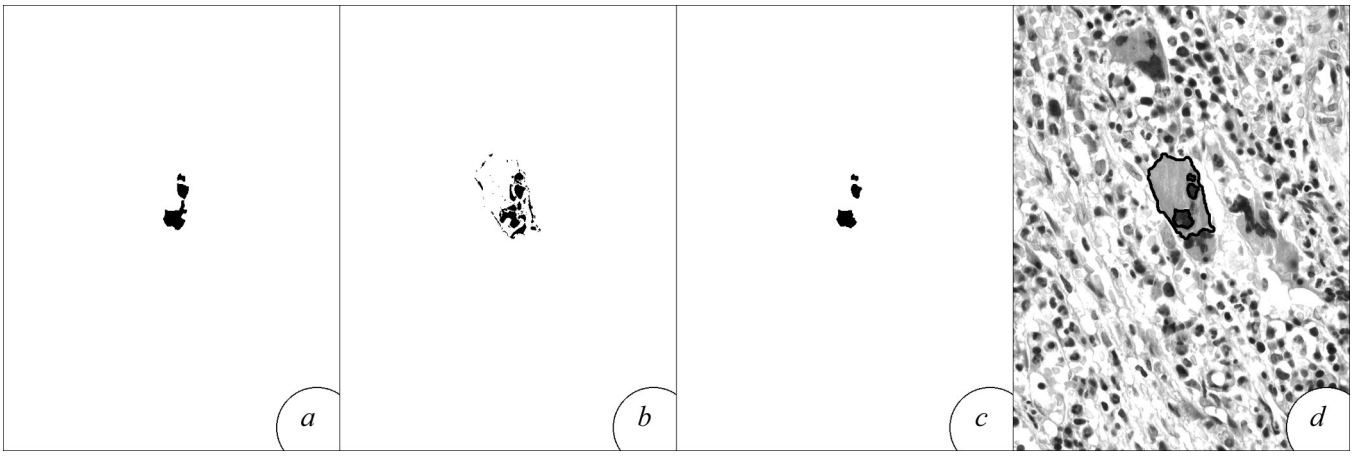

Fig. 2. The nucleus already obtained by mathematical morphology **(a)** is completed by the result of the wavelet analysis **(b)**. The contour of the enhanced nucleus **(c)** has been superimposed on the input image **(d)**.

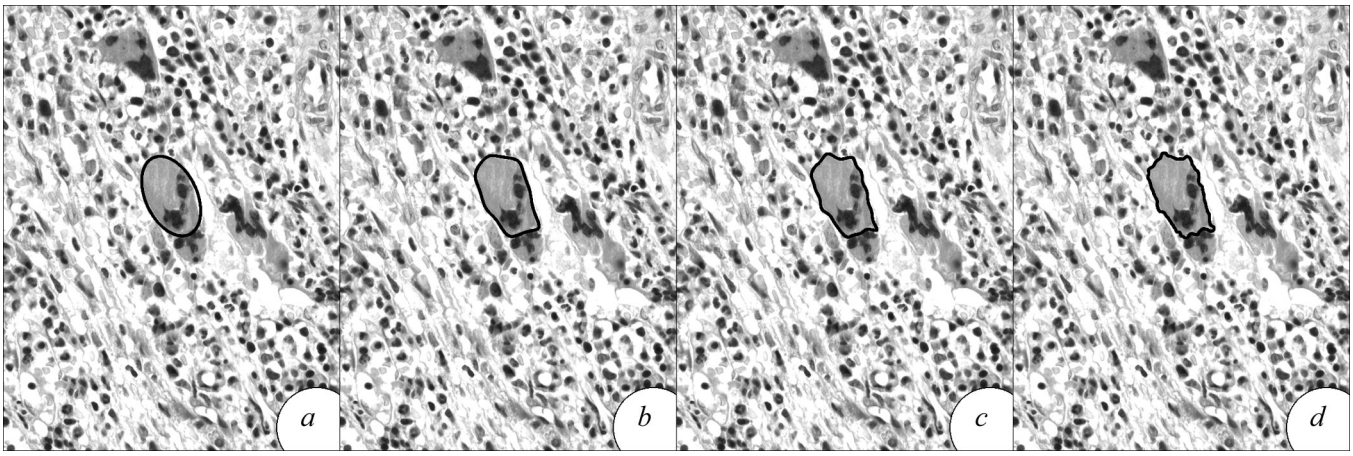

Fig. 3. Reconstruction of the contour of the cell by the inverse elliptic fourier transform. Many harmonics are necessary to get fine details. In this example we have computed 1 **(a**), 7 **(b)**, 15 **(c)** and 50 **(d)** harmonics.

features $\{f_2, f_3, f_6, f_8, f_9, f_{10}, f_{11}\}$ are appropriate for discriminating between the cases of essential thrombocythemia and idiopathic myelofibrosis with sensitivities equal to S_{ET}=0.8820 and to S_{IMF}=0.9023. In order to validate the correctness of the new classifier, its output was compared with the morphological photo-interpretation provided by the pathologists for the whole

Table 2. Optimal confusion matrices obtained with features $\{f_1, f_2, f_{11}\}$ for pathological and normal megakaryocytes (left) and with features $\{f_2, f_3, f_8, f_9, f_6, f_{10}, f_{11}\}$ for essential thrombocythemia and idiopathic myelofibrosis (right).

$$\begin{bmatrix} 98.4\% & 1.6\% \\ 2.9\% & 97.1\% \end{bmatrix} \quad \begin{bmatrix} 91.7\% & 8.3\% \\ 13.8\% & 86.2\% \end{bmatrix}$$

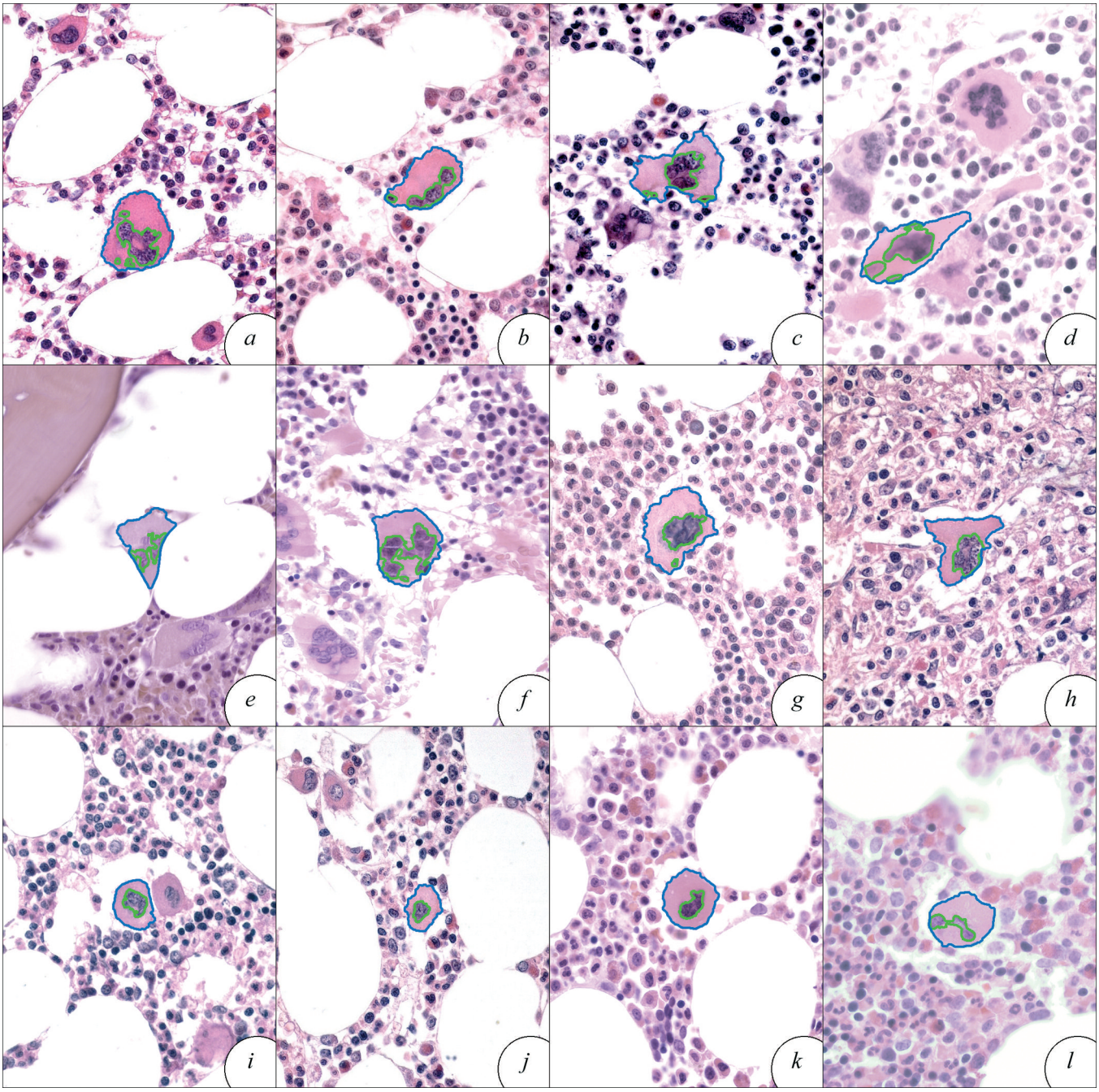

Fig. 4. Examples of segmentation in the cases of essential thrombocythemia **(a-d)**, idiopathic myelofibrosis **(e-h)** and normal megakaryocytes **(i-l)**.

database. The software considered each given cell as unclassified and then classified it by comparing its features with those of the remaining cells. This process was repeated for every single cell and therefore the results have to be considered on average.

The results so far obtained are encouraging. Nevertheless we are going to enhance the performance of the classifier via an improved segmentation procedure and different clustering algorithms

Discussion

The diagnosis of chronic myeloproliferative disorders requires a multidisciplinary approach which includes bone marrow biopsy evaluation (Thiele et al., 2000; Kreft et al., 2005). Morphological features play an essential role not only in making a diagnosis but also in identifying risk groups and assessing prognostic factors (Chait et al., 2005). A challenging point is the discrimination between the thrombocythemic prefibrotic phase of chronic idiopathic myelofibrosis (CIMF) and other disorders with thrombocythemia (PV and ET) as these conditions are characterized by a different evolution in terms of complications like venous thrombosis, development of fibrosis and leukemic transformation and therefore require different therapeutic approaches (Thiele et al., 1996, 2001b; Harrison et al., 2005). In CMPDs high platelet counts in the peripheral blood are sustained by the increase in megakaryopoiesis. The proliferative "stress" seems to be often moderate and ever counterbalanced by the maturation of the megakaryocytes (Thiele et al., 1999a). This is well proved by the morphological and morphometric evaluation of megakaryocytes and by the immunohistochemical analysis of the bone marrow parenchyma. Immunohistochemical evaluation of BMBs in CMPDs has assumed an ever-increasing value in the differentiation of "borderline" cases in which morphology alone is not sufficient to achieve a diagnosis (Florena et al., 2004). Evaluation of the neoangiogenesis, overall microvessel density and distribution of $CD34^+$ cells may add a valuable amount of information concerning the status of the hematopoietic parenchyma (Mesa et al., 2000; Thiele et al., 1999b, 2001b; Thiele and Kvasnicka, 2003b). Among the histologic criteria, megakaryocyte morphologic features like number, size and form proved to be the most crucial point able to distinguish the different Ph- CMPDs. Multiple parameters can be easily assessed by the evaluation of standard hematoxylin-eosin sections which can be useful in achieving the correct diagnosis of CMPD. In ET the bone marrow parenchyma often appears normocellular with no left-shifting of the myeloid and erythroid cell lines. MKCs in ET are single or loosely clustered large to giant mature cells with deeply lobulated staghorn-like nuclei while PV shows pleomorphous MKCs and in prefibrotic CIMF more frequent clusters of abnormal MKCs of different size with abnormal maturation and hypo-lobulated cloud-like nuclei are characteristic (Thiele et al., 1999c). In a recent study, the determination of the clustering index (i.e. the tendency of megakaryocytes to form clusters) was found to be low in ET while it was higher in CIMF increasing along with progression of fibrosis (Florena et al., 2004).

Mathematical morphology is widely used to extract or suppress image structures with apriori known shape, size and orientation and to achieve a variety of processing tasks. This approach is well known and robust, but usually sensitive to the change of luminosity. Therefore a preprocessing phase was necessary to normalize the hue/saturation of the photomicrographs via an extensive statistical examination of the database. Though the shape of the cell so obtained was normally well defined, we applied a wavelet transform to further improve the contour of the nucleus. Wavelets provide an alternative approach, which can be thought of as a generalization of the Gabor transform, to signal processing and constitute a link between mathematics, physics and electrical engineering. Among several discrete implementations for wavelet analysis, we chose the *à trous* algorithm which can be seen as a filter bank process. The efficiency of the classifier has been verified with a set of different features which describe each megakaryocyte. The elliptic Fourier transform was used to estimate the complexity of the contour of the cell (Nafe et al., 1992). In particular, we experimentally verified that two sets of such features are better than others when discriminating between pathological and normal megakaryocytes rather than essential thrombocythemia and idiopathic myelofibrosis.

We decided to analyze morphometrically cytoplasmic and nuclear features like size and shape proving experimentally that it is possible to successfully classify particular classes of human megakaryocytes by using morphometric information. According to morphology, normal or reactive megakaryocytes are normal-sized cells with lobulated nuclei and no gross cytological abnormalities; on the other hand, megakaryocytes in ET are large to giant cells with deeply lobulated staghorn nuclei. Morphometric data reflect well these morphological findings and, summarizing, features related to the general contour of the cell like cytoplasmic area and perimeter and difference between the contour of the cell and its reconstructed one are able to discriminate between normal or reactive MKCs and pathological ones, while for the differential diagnosis of ET and IMF nuclear features as well as cell global circularity are better indicators. The results so far obtained are encouraging. Nevertheless we are going to enhance the performance of the classifier via an improved segmentation procedure and different clustering algorithms. Previous works on the automatic analysis of cells required a hand-made segmentation. Although all threshold values have been predetermined on the basis of apriori information or can be computed automatically, that is the whole algorithm is unsupervised, we want to stress that our method

should be considered as a fast preprocessing tool to help experts during the diagnosis phase. Moreover, it is noteworthy that the features and the methodologies here introduced are general and can be extended to solve different object recognition problems.

Appendix A

Morphological operators are widely used to extract or suppress image structures with apriori known shape, size and orientation. This information is embedded by a so called structuring element SE, which represents the range of the operators. Practically, the operators test whether their structuring element fits or does not fit the objects present in the image. Elementary morphological operators can be effectively combined to achieve important image processing tasks.

Let us define the erosion ε and the dilation δ of an image I with grey levels in [0, 255] and the flat structuring element Dr obtained as the approximated discrete disk of radius r:

$$\varepsilon_r\left(I\left(\underline{p}\right)\right) = \min_{\underline{q} \in D_r} I\left(\underline{p}+\underline{q}\right) \text{ and } \delta_r\left(I\left(\underline{p}\right)\right) = \max_{\underline{q} \in D_r} I\left(\underline{p}+\underline{q}\right)$$

In general both erosion and dilation are not invertible, but we can define two morphological operators, called opening γ and closing ϕ, which should recover as much as possible the original image I:

$$\gamma_r(I) = \delta_r\left(\varepsilon_r(I)\right) \quad \text{and} \quad \varphi_r(I) = \varepsilon_r\left(\delta_r(I)\right)$$

The usual application of the opening is the removing of small objects from I, while preserving the shape and size of larger objects. Viceversa the closing fills in the smaller gaps in I. The opening and closing can be combined to enhance the contrast of I by using the following formula:

$$ec_r(I) = \max\left\{0,\ \min\left\{255,\ I + \max\left\{0,\ I - \gamma_r(I)\right\}\right\} - \max\left\{0,\ \varphi_r(I) - I\right\}\right\}$$

All these operators hold for binary images, too. In the case of binary images, the contour of an object X can be easily defined as:

$$\partial(X) = \delta_1(X) \cap X^c$$

The morphological part of the segmentation process can be sketched by the following sequence of main operations (Fig. 1):

a. $I' \leftarrow ec_1\left(\delta_1(I)\right)$;

b. $I_{cyto} \leftarrow \left\{I' : \tau_1 \le I' \le \tau_2\right\}$; $I_{cyto} \leftarrow \left\{I_{cyto} : \left|I_{cyto}\right| \ge 3000\right\}$;

c. $I_{cell} \leftarrow \left\{I' : I' < \tau_2\right\} \cap I_{cyto}$;

d. $I_{cyto} \leftarrow \left(\left\{I' : I' \ge \tau_2\right\} \cap \left\{I_{cell} \cap I_{cyto}^c\right\}\right) \cup I_{cyto}$;

e. $I_{nucl} \leftarrow I_{cell} \cap I_{cyto}^c$; $I_{nucl} \leftarrow \left\{I_{nucl} : \left|I_{nucl}\right| \ge 100\right\}$;

f. $I_{nucl} \leftarrow \left\{I_{nucl} : \left|\partial(I_{nucl}) \cap I_{cell}\right| / \left|\partial(I_{nucl})\right| \ge 0.7\right\}$;

g. $I_{cell} \leftarrow \varphi_4\left(\gamma_4\left(I_{cell}\right)\right)$;

h. $I_{cell} \leftarrow \left\{I_{cell} : \min \left\| I_{cell} - \text{center}(1) \right\|\right\}$.

It must be noted that all radii of the structuring elements have been experimentally chosen according to the size of the input images.

Appendix B

Let us assume that a coarse approximation I^i of the input image $I=I_0$ can be written as an infinite scalar product of finer and finer approximations with a high-pass filter h:

$$I_i\left(\underline{p}\right) = \sum_{\underline{q} \in D_\infty} h_{\underline{q}} I_{i-1}\left(\underline{p} + 2^{i-1}\underline{q}\right)$$

On the contrary, the wavelet coefficient W_i can be obtained by convolving with a low-pass filter l:

$$W_i\left(\underline{p}\right) = \sum_{\underline{q} \in D_\infty} l_{\underline{q}} I_{i-1}\left(\underline{p} + 2^{i-1}\underline{q}\right)$$

That is, each wavelet image W_i has the same number of pixels as I_0. Moreover the distance between samples increases by a factor 2 from plane i to i+1, since the convolution is done by keeping one pixel out of two. This means that in practice the size of h and l doesn't increase, whatever the level i of the scale is.

We have preferred a linear interpolation to define the kernel of the high-pass filter h:

$$h = \frac{1}{16}\begin{pmatrix} 1 & 2 & 1 \\ 2 & 4 & 2 \\ 1 & 2 & 1 \end{pmatrix}$$

because it is isotropic and limited to just 9 elements. The simplest choice for the low-pass filter l is the difference between two consecutive resolutions:

$$W_i = I_{i-1} - I_i$$

Small objects are enhanced in the first planes, while big components are located in the last planes. Pointlike details and the background are more evident in W_1. Moreover, bright structures are exalted by positive values, while dark regions are put in evidence by negative values. Therefore, the absolute value of the first 4 coefficient planes retain most structures of the nucleus: the combination of these binaryzed images improves the shape of the nucleus already extracted by mathematical morphology (Fig. 2):

$$I_{nucl} \leftarrow \left(\bigcup_{i=1}^{4}\left\{T_i : T_i \ge \max(T_i)/3\right\}\right) \cup I_{nucl} \quad \text{where} \quad T_i \leftarrow I_{cell} \cap \text{abs}(W_i)$$

Finally, to complete the extraction of the nucleus we smooth its contour by mathematical morphology:

$$I_{nucl} \leftarrow \varphi_4\left(\gamma_4\left(I_{nucl}\right)\right)$$

Appendix C

A closed contour of k points and Euclidean length L can be identified by four Fourier coefficients a_n, b_n, c_n and d_n of N harmonics:

$$a_n = \frac{L}{2n^2\pi^2}\sum_{i=1}^{k}\frac{dx_i}{dt_i}\left(\cos\frac{2n\pi t_i}{L} - \cos\frac{2n\pi t_{i-1}}{L}\right),$$

$$b_n = \frac{L}{2n^2\pi^2}\sum_{i=1}^{k}\frac{dx_i}{dt_i}\left(\sin\frac{2n\pi t_i}{L} - \sin\frac{2n\pi t_{i-1}}{L}\right),$$

$$c_n = \frac{L}{2n^2\pi^2}\sum_{i=1}^{k}\frac{dy_i}{dt_i}\left(\cos\frac{2n\pi t_i}{L} - \cos\frac{2n\pi t_{i-1}}{L}\right),$$

$$d_n = \frac{L}{2n^2\pi^2}\sum_{i=1}^{k}\frac{dy_i}{dt_i}\left(\sin\frac{2n\pi t_i}{L} - \sin\frac{2n\pi t_{i-1}}{L}\right).$$

From a geometrical point of view a_i and b_i (c_i and d_i) represent the projection on the x (y) axes of the semimajor and of the semiminor axis of the ith harmonic.

The inverse process recovers the ith pixel of the contour from the harmonics:

$$X_i = \sum_{n=1}^{N}\left(a_n\cos\frac{2n\pi t_i}{L} + b_n\sin\frac{2n\pi t_i}{L}\right)$$

$$Y_i = \sum_{n=1}^{N}\left(c_n\cos\frac{2n\pi t_i}{L} + d_n\sin\frac{2n\pi t_i}{L}\right)$$

The total complexity of the contour can be estimated by comparing the original and reconstructed contours through the following measure:

$$d = \frac{1}{k}\sum_{i=1}^{k}\left\|(x_i, y_i) - (X_i, Y_i)\right\|$$

which takes into account the distance between each point of the contour and its reconstructed one. It is quite obvious that the smoother the original contour is, the fewer harmonics will be necessary to correctly reconstruct it.

Acknowledgements. The Committee for Scientific Research of the Republic of Poland, through grant no 3 P05B 084 24, has supported Dr. Rudzki in this work. This paper has been partially supported by a grant of MIUR 60%, Rome.

References

Altman D. (1999). Practical statistics for medical research. Chapman & Hall/CRC. Boca Raton. Florida.

Beksaç M., Beksaç M.S., Tipi V.B., Duru H.A., Karakas M.U. and Çakar A.N. (1997). An artificial intelligent diagnostic system on differential recognition of hematopoietic cells from microscopic images. Cytometry 30, 145-150.

Chait Y., Condat B., Cazals-Hatem D., Rufat P., Atmani S., Chaoui D., Guilmin F., Kiladjian J.J., Plessier A., Denninger M.H., Casadevall N., Valla D. and Briere J.B. (2005). Relevance of the criteria commonly used to diagnose myeloproliferative disorder in patients with splanchnic vein thrombosis. Br. J. Haematol. 129, 553-560.

Chui C. (1992). An introduction to wavelets, wavelet analysis and its applications. Academic Press. San Diego. California.

Coelho R.C., Di Gesù V., Lo Bosco G., Tanaka J.S. and Valenti C. (2002). Shape-based features for cat ganglion retinal cells classification, real-time imaging, special issue on imaging in bioinformatics. Academic Press 8, 213-226.

Cohen A. and Kovasevic J. (1996). Wavelets: The mathematical background. Proc. IEEE 8, 514-522.

Daubechies I. (1992). Ten lectures on wavelets. CBMS-NSF Regional Conference Series on Applied Mathematics. Society for Industrial and Applied Mathematics. Philadelphia. Pennsylvania. 61.

Florena A.M., Tripodo C., Iannitto E., Porcasi R., Ingrao S. and Franco V. (2004). Value of bone marrow biopsy in the diagnosis of essential thrombocythemia. Haematologica 89, 911-919.

Graps A. (1995). An introduction to wavelets. IEEE Computational science and engineering. Los Alamitos, California, 2, 1-18.

Grossmann A. and Morlet J. (1984). Decomposition of Hardy functions into square integrable wavelets of constant shape. SIAM J. Math. Anal. 15, 723-736.

Harrison C.N., Campbell P.J., Buck G., Wheatley K., East C.L., Bareford D., Wilkins B.S., van der Walt J.D., Reilly J.T., Grigg A.P., Revell P., Woodcock B.E., Green A.R. and United Kingdom Medical Research Council Primary Thrombocythemia 1 Study (2005). Hydroxyurea compared with anagrelide in high-risk essential thrombocythemia. N. Engl. J. Med. 353, 33-45.

Holschneider M., Kronland-Martinet R., Morlet J. and Tchamitchian Ph. (1988). The à trous Algorithm. Publication CPT-88/P.2215. Marseille, 1-22.

Kreft A., Buche G., Ghalibafian M., Buhr T., Fischer T., Kirkpatrick C.J. (2005). The incidence of myelofibrosis in essential thrombocythaemia, polycythaemia vera and chronic idiopathic myelofibrosis: a retrospective evaluation of sequential bone marrow biopsies. Acta Haematol. 113, 137-143.

Kuhl F.P. and Giardina C.R. (1982). Elliptic fourier feature of a closed contour. Computer graphics and image processing 18, 236-258.

Kvasnicka H.M., Thiele J., Schroeder M., von Loesch C., Diehl V. (2004). Bone marrow angiogenesis - methods of quantification and changes evolving in chronic myeloproliferative disorders. Histol. Histopathol. 19, 1245-1260.

Mallat S.G. (1989). A theory for multiresolution signal decomposition: the wavelet representation. IEEE Trans. PAMI 11, 674-693.

Mesa R.A., Hanson C.A., Rajkumar V., Schroeder G. and Tefferi A. (2000). Evaluation and clinical correlations of bone marrow angiogenesis in myelofibrosis with myeloid metaplasia. Blood 96, 3374-3380.

Mesa R.A., Hanson C.A., Li C.Y., Yoon S.Y., Rajkumar V., Schroeder G. and Tefferi A. (2002). Diagnostic and prognostic value of bone marrow angiogenesis and megakaryocyte c-Mpl expression in essential thrombocythemia. Blood 99, 4131-4137.

Michiels J.J. and Thiele J. (2002). Clinical and pathological criteria for the diagnosis of essential thrombocythemia, polycythemia vera and idiopathic myelofibrosis (agnogenic myeloid metaplasia). Int. J. Hematol. 76, 133-145.

Nafe R., Kaloutsi V., Choritz H. and Georgii A. (1992). Elliptic Fourier analysis of megakaryocyte nuclei in chronic myeloproliferative disorders. Anal. Quant. Cytol. Histol. 14, 391-397.

Ohshima K., Kikuchi M. and Takeshita M. (1995). A megakaryocyte analysis of the bone marrow in patients with myelodysplastic syndrome, myeloproliferative disorder and allied disorders. J. Pathol. 177, 181-189.

Schafer A.I. (2004). Thrombocytosis. N. Engl. J. Med. 350, 1211-1219.

Shensa M.J. (1992). Discrete wavelet transforms: Wedding the à trous and mallat algorithms. IEEE Trans. Signal Processing 40, 2464-2482

Soille P. (2003). Morphological image analysis. 2nd ed. Springer-Verlag. New York.

Thiele J. and Kvasnicka H.M. (2003a). Chronic myeloproliferative disorders with thrombocythemia: A comparative study of two classifiaction systems (PVSG, WHO) on 839 patients. Ann. Hematol. 82, 148-152.

Thiele J. and Kvasnicka H.M. (2003b). Diagnostic differentiation of essential thrombocythaemia from thrombocythaemias associated with chronic idiopathic myelofibrosis by discriminate analysis of bone marrow features - a clinicopathological study on 272 patients. Histol. Histopathol. 18, 93-102.

Thiele J., Kvasnicka H.M., Werden C., Zankovich R., Diehl V. and Fischer R. (1996). Idiopathic primary osteo-myelofibrosis: a clinico-pathological study on 208 patients with special emphasis on evolution of diseases features, differentiation from essential thrombocythemia and variables of prognostic impact. Leuk. Lymphoma 22, 303-317.

Thiele J., Kvasnicka H.M. and Fischer R. (1999a). Histochemistry and morphometry on bone marrow biopsies in chronic myeloproliferative disorders - aids to diagnosis and classification. Ann. Hematol. 78, 495-506.

Thiele J., Kvasnicka H.M., Diehl V., Fischer R. and Michiels J. (1999b). Clinicopathological diagnosis and differential criteria of thrombocythemias in various myeloproliferative disorders by histopathology, histochemistry and immunostaining from bone marrow biopsies. Leuk. Lymphoma 33, 207-218.

Thiele J., Kvasnicka H.M., Boeltken B., Zankovich R., Diehl V. and Fischer R. (1999c). Initial (prefibrotic) stages of idiopathic (primary) myelofibrosis (IMF) - a clinicopathological study. Leukemia 13, 1741-1748.

Thiele J., Kvasnicka H.M., Zankovich R. and Diehl V. (2000). Relevance of bone marrow features in the differential diagnosis between essential thrombocythemia and early stage idiopathic myelofibrosis. Haematologica 85, 1126-1134.

Thiele J., Imbert M., Pierre R., Vardiman J.W., Brunning R.D. and Flandrin G. (2001a). Chronic idiopathic myelofibrosis. WHO classification of tumours: tumours of haematopoietic and lymphoid tissues. IARC Press. Lyon. 35-38.

Thiele J., Kvasnicka H.M., Zankovich R. and Diehl V. (2001b). Clinical and morphological criteria for the diagnosis of prefibrotic idiopathic (primary) myelofibrosis. Ann. Hematol. 80, 160-165.

Thiele J., Kvasnicka H.M., Zankovich R. and Diehl V. (2002). Early-stage idiopathic (primary) myelofibrosis - current issues of diagnostic features. Leuk. Lymphoma 43, 1035-1041.

Thiele J., Kvasnicka H.M. and Diehl V. (2005a). Initial (latent) polycythemia vera with thrombocythemia mimicking essential thrombocythemia. Acta Haematol. 113, 213-219.

Thiele J., Kvasnicka H.M., Zankovich R. and Diehl V. (2005b). Bone marrow $CD34^+$ progenitor cells in Philadelphia chromosome-negative chronic myeloproliferative disorders - A clinicopathological study on 575 patients. Leuk. Lymphoma 46, 709-715.

Accepted February 15, 2006